Colloid Polym Sci (2009) 287:533–540
DOI 10.1007/s00396-009-1999-y

ORIGINAL CONTRIBUTION

Study on luminescence characteristic of the ZnO/polymer hybrid films

Qian-huo Chen · Shi-yong Shi · Wen-gong Zhang

Received: 24 February 2008 / Revised: 9 November 2008 / Accepted: 7 January 2009 / Published online: 22 January 2009

Abstract The cyclohexane solution of PS (polystyrene) and the ethyl acetate solution of PMMA (polymethyl methacrylate) were used as flowing liquid; the ZnO/polymer hybrid colloids were successively produced by focused pulsed laser ablation of ZnO target in interface of solid and flowing liquid. As solvent in the hybrid colloids has volatized, the ZnO/polymer hybrid films were obtained. The hybrid colloids were characterized by high-resolution transmission electron microscopy (HRTEM) and select-area electron diffraction (SEAD). The results show a good dispersion of the ZnO nanoparticles in the polymer matrix. The hybrid films were characterized by fluorescence spectrum, Fourier transform infrared spectroscopy (FTIR) spectroscopy, thermogravimetry with FTIR (TG/FTIR), and X-ray photoelectron spectrum. The results show the ZnO/polymer hybrid films can radiate strong blue light under ultraviolet. Meanwhile, the ZnO/polymer hybrid films have higher chemical stability than ZnO nanoparticles because nano-ZnO nanoparticles were enwrapped by polymers. In addition, the ZnO hybrid films have higher thermal stability then the related pure polymers because of strong interaction among ZnO nanoparticles and polymers.

Keywords ZnO nanoparticles · Pulsed laser ablation · Colloids · Polymer · Hybrid film · Fluorescence

Q.-h. Chen (✉) · S.-y. Shi · W.-g. Zhang
College of Chemistry and Materials Science,
Fujian Normal University,
Fuzhou 350007, People's Republic of China
e-mail: qhchen@fjnu.edu.cn

Introduction

Zinc oxide (ZnO) is an odd material facing novel applications due to its optical, electrical, and structural properties [1]. Nanocomposite ZnO thin film possesses many special features and has been used in many important fields [2, 3]. ZnO is a semiconductor with wide bandgap (3.2–3.5 eV) that makes it a promising material for photonics application in the ultraviolet (UV) and blue region of the electromagnetic spectrum. The high exciton-binding energy (60 meV) allows efficient excitonic emission even at room temperature [1, 4, 5].

Hybrid materials consisting of zinc oxide and polymers exhibit the merits of good properties of zinc oxide and well mechanic processing, easy flexibility of polymer. Especially, hybrid materials consisting of soluble polymers with excellent mechanical properties and nice filming can be used in large area and flat panel displays and to make polymer light-emitting diodes (PLED).

Up to now, the main synthetical methods for preparation of the hybrid materials are in situ dispersion polymerization process, blend process, intercalation process, and sol–gel process [6]. But the problems of well-distribution of nano-ingredients in the hybrid materials have not been completely resolved, and have already become the technological bottleneck for the researching and application of inorganic nano/organic polymer functional materials.

Recently, we have applied a pulsed laser to ablate metal oxide target immersed in a flowing liquid to successively prepare metal oxide organic colloids [7–12]. If a solution of polymer is used as flowing liquid, metal oxide/polymer hybrid colloids can be obtained, and the polymer solution containing metal oxide nanoparticles can be used to obtain large area luminescent film by spin coating procedure [13].

In this paper, nano-ZnO/polymer hybrid colloids were obtained by focused pulsed laser ablation of ZnO target immersed in the cyclohexane solution of 0.5% PS (polystyrene) and ethyl acetate solution of 0.5% polymethyl methacrylate (PMMA). As solvent in the hybrid colloids has volatilized, nano-ZnO/PS and ZnO/PMMA hybrid film with good distribution and stability of nano-ZnO nanoparticles were obtained. High-resolution electron micrographs (HRTEM), select-area electron diffraction (SEAD), fluorescent spectra, Fourier transform infrared spectroscopy (FTIR), thermogravimetry with FTIR (TG/FTIR), and X-ray photoelectron spectroscopy (XPS) were used to characterize the hybrid films.

Experimental methods and materials

The cyclohexane solution of 0.5% PS and ethyl butyrate solution of 0.5% PMMA were used as flowing liquids. The ZnO target was irradiated by the focused laser beam with 532 nm from DCR-3G Nd:YAG laser (Spectra Physics), operating at 10 Hz, at the fluence of 200 mJ/pulse with pulse width of 8 ns. The spot size of the laser beam on the surface of target was about 1 mm, and the flowing liquid flowed over the target at the speed of about 0.05 mL/s. The ZnO target was submerged at the depth of 1–2 mm. The whole preparation process was done in a high pure nitrogen atmosphere. The obtained colloids were concentrated and dropped on the clean glass slides. As solvent in colloids volatilized, the decorated nano-ZnO/PS and ZnO/PMMA hybrid films were obtained.

The ZnO–polymer films were prepared by blend process. The nano-ZnO powder with particle size of 300–500 nm was dissolved in ethyl acetate solution of PMMA (0.5%) and cyclohexane solution of PS (0.5%). The ZnO–polymer film was prepared by dropping the organic solutions onto clear glass slides. The solvent was allowed to evaporate in air at room temperature.

The HRTEM photographs and SEAD were obtained on the FEI F20 transmission electron microscope (Philips Company). Ten drops of obtained colloids were deposited on a copper mesh coated with an amorphous carbon film for HRTEM observation. The fluorescence spectra of obtained films were measured by an Edinburgh FL/FS 920 fluorophotometer (input slit widths=0.9 nm, output slit widths=1.8 nm). FTIR was performed on an AVATA 360 FT-IR spectrometer (Thermo Fisher Scientific), and attenuated total reflection (ATR) sampling technique was used to analyze the hybrid films. TG/FTIR analyses were performed on a Mettler Toledo TGA/SDTA 851^e and Nicolet 5700 FT-IR; TG measurements were performed at 10 °C/min scanning rate, employing a 50 mL/min flow of dry nitrogen as a purge gas for the sample and reference sells. X-ray photoelectron spectroscopy (XPS) was performed on a PHI Quantum 2000 Scanning ESCA Microprobe (Physical Electronics Company). The instrument was operated at about 5×10^{-8} Pa using a 1,486.6-eV $K\alpha$ aluminum X-ray source. The input lens of the photoelectron analyzer was configured in such a way that the sample diameter is of approximately 200 μm.

Results and discussion

HRTEM analysis

In the case of preparing the ZnO nanoparticles in polymer materials, it is interesting to investigate the morphology and distribution of the ZnO nanoparticles in the matrix. Because the origin ZnO nanoparticles produced by pulsed laser ablation are highly reactive due to many dangling bonds on the surface, the ZnO nanoparticles easily aggregate and form bigger particles. The polymers can be used to control the growth rate as well as to stabilize the ZnO nanoparticles. Figure 1a shows the HRTEM micrograph of the ZnO/PMMA colloids after being prepared for 1 h. The ZnO nanoparticles are well distributed in the PMMA matrix. The diameter of the ZnO nanoparticles in the PMMA matrix is from several nanometers to 60 nm. In order to study the microstructure of the nanoparticle and get clear image, a bigger nanoparticle is selected. As can be seen from Fig. 1b, the particle with the size of 40 nm appears as a regular crystalline lattice superimposed on an amorphous background due to the carbon support and the PMMA matrix. The nature of the crystalline phase of the particle can be determined by the select-area electron diffraction (SEAD) pattern (Fig. 1c). The measured inter-reticular distances (0.24 and 0.14 nm) are in perfect agreement with those of JCPDS card (80-0075). The inter-reticular distances of the (1 0 1) and (1 1 2) planes are d_{101}= 0.247 and d_{112}=0.138 nm. The conclusion can be obtained that the structure of the particle in Fig. 1b is hexagonal with cell parameters consistent with those in JCPDS card (80-0075).

In the presence of PS matrix, the similar results can be obtained. Figure 2a shows the HRTEM micrograph of the ZnO/PS colloids after being prepared for 1 h. The HRTEM image shows a good dispersion of the ZnO nanoparticles in the PS matrix. The particle with the size of 60 nm in Fig. 2b appears as a regular crystalline lattice superimposed on an amorphous background due to the carbon support and the PS matrix. Figure 2c shows the select-area electron diffraction (SEAD) pattern of Fig. 2b. The measured inter-reticular distances (0.26 nm) are in perfect agreement with those of JCPDS card (80-0075). The inter-reticular distances of the (0 0 2) is d_{002}=0.260 nm. The conclusion can

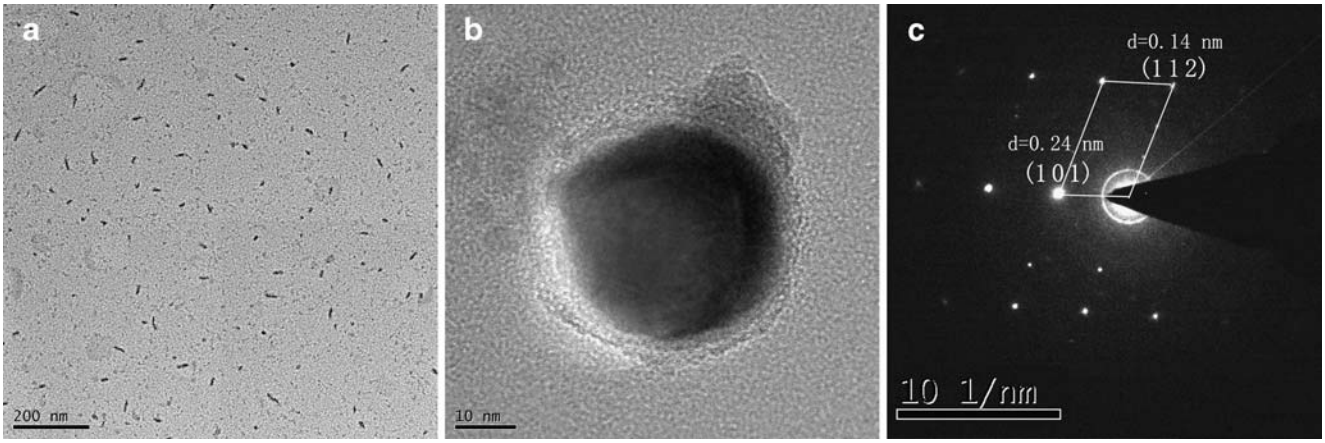

Fig. 1 HRTEM image (**a**), single bigger nanoparticles images (**b**) of the ZnO/PMMA colloids and the select-area electron diffraction (SEAD) pattern of (**b**). The *scale bars* in (**a**), (**b**), and (**c**) are 200 nm, 10 nm, and 10 1/nm, respectively

be obtained that the structure of the particle in Fig. 2b is hexagonal with cell parameters consistent with those in JCPDS card (80-0075).

FTIR analysis of the ZnO/polymer hybrid film

Figure 3 shows the FT-IR spectra of the ZnO/PMMA hybrid film and standard FT-IR spectrum of PMMA from the library of Aldrich condensed phase supplement. Using Omnic 7.2 (Thermo Electron corporation), the match value of these two spectra is as high as 85.6%, which indicates the main component of hybrid film is PMMA. Thus, the conclusion can be obtained that PMMA locates at the surface of the hybrid films. In the FTIR spectrum of the ZnO/PMMA, the peak at 1,727.7 cm^{-1} is due to the carboxyl stretching vibration. This peak shift to short wavenumber compared to that of the standard PMMA FT-IR spectrum. The main reason is that PMMA can coordinate with Zn^{2+} ions in the surface of the ZnO particles and form delocalized π bonds [14]. As a result, the electron density and force parameter of C=O bond in PMMA are decreased.

Figure 4 shows the FTIR spectra of the ZnO/PS hybrid film and standard FT-IR spectrum of PS from library of HR Aldrich FT-IR collection edition II. Using Omnic 7.2, the match value of these two spectra is as high as 89.8%, which indicates the main component of the material detected by FTIR is PS. Similarly, the conclusion that PS locates at the surface of the ZnO/PS hybrid films can be obtained.

Fluorescence spectrum of the ZnO/polymer hybrid film

The two kinds of ZnO/polymer hybrid films prepared by pulsed laser ablation can emit intense blue light under UV radiations. Figure 5 shows the fluorescence spectrum of the ZnO/PMMA hybrid film, and the inset shows the Gaussian fit curves of the emission spectrum. It is found that the ZnO/PMMA hybrid film has a strong broad excitation peak at 382 nm, a weak absorption peak at about 301 nm, and

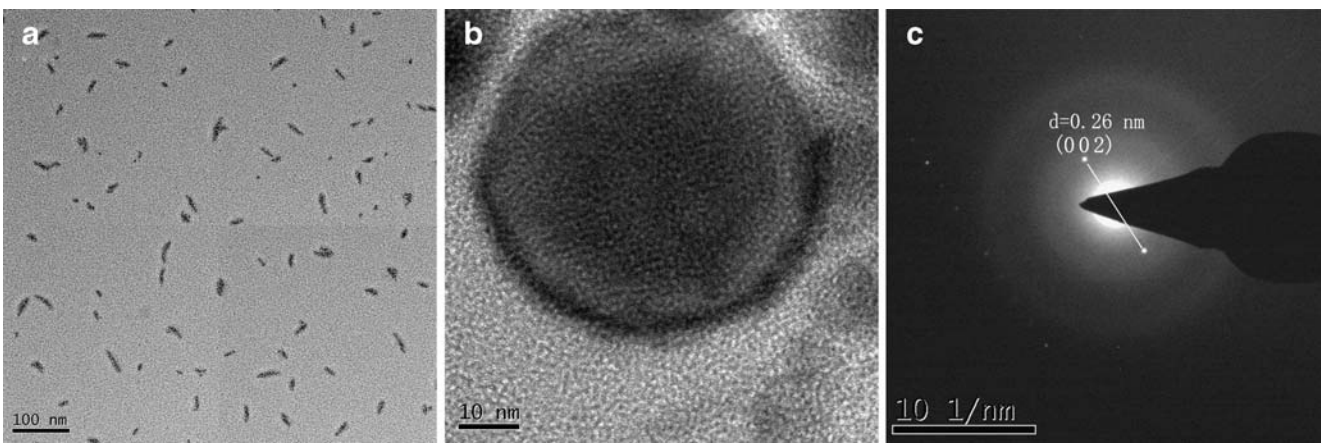

Fig. 2 HRTEM images (**a**), single bigger nanoparticles images (**b**) of the ZnO/PS colloids and the select-area electron diffraction (SEAD) pattern of (**b**). The *scale bars* in (**a**), (**b**), and (**c**) are 100 nm, 10 nm, and 10 1/nm, respectively

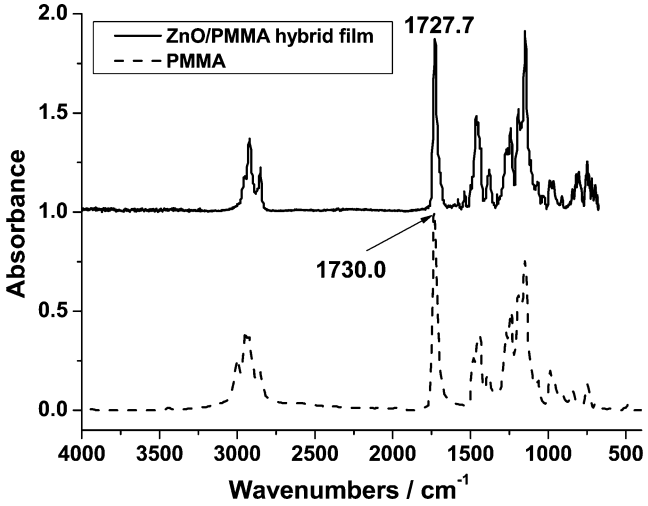

Fig. 3 FTIR spectra of the ZnO/PMMA hybrid film and PMMA from library of Aldrich condensed phase supplement

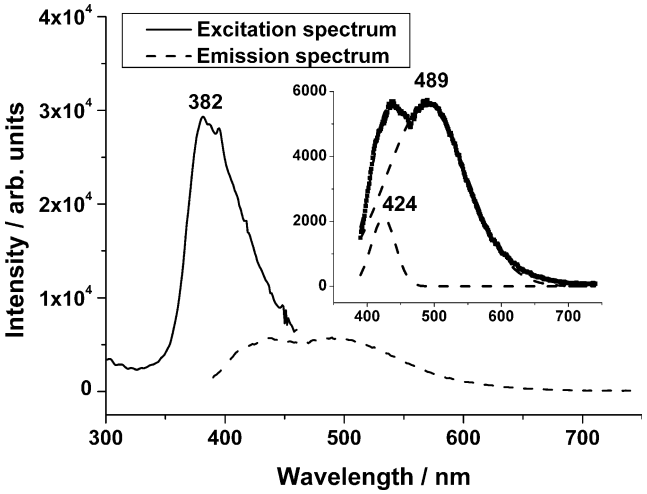

Fig. 5 Fluorescence spectrum of the ZnO/PMMA hybrid film; the *inset* is the Gaussian fit curve of the emission spectrum

two emission peaks located at 424 and 489 nm, respectively. As reported in the literature [11], the excitation peaks of the ZnO ethanol colloids locate at 272, 311, and 346 nm, respectively. Therefore, the excitation peak at 382 nm of the ZnO/PMMA hybrid film can be attributed to the $\pi \rightarrow \pi^*$ transition of the PMMA; the weak excitation peak at 301 nm can be attributed to electron transition of the ZnO particles. The emission peak at 424 nm can be attributed to electron-hole plasma recombination emission of ZnO nanoparticles [15], and the singly ionized oxygen vacancy is responsible for the blue emission at 489 nm; this emission results from the recombination of a photogenerated hole with the singly ionized charge state of the defect [16, 17]. These findings confirm that two different luminescence mechanisms exist in ZnO/PMMA hybrid film and energy transfers from PMMA to ZnO particles. One mechanism is electron-hole plasma recombination emission of ZnO particles; another is related to oxygen vacancy. PMMA absorbs the UV energy and transfers it to ZnO particles. ZnO particles receive the energy from PMMA and emit strong blue emission at 489 nm. Two different mechanisms also confirm two different ZnO particles existing in the ZnO/PMMA hybrid film. These two ZnO particles may be ZnO nanoparticles and decorated ZnO particles with surface Zn^{2+} coordinated by PMMA. Because the power density of the pulsed laser beam in the focus spot is as high as 10^8 W/cm^2, the obtained ZnO nanoparticles are highly reactive due to many dangling bonds on its surface, and the C=O in the PMMA can coordinate with the surface zinc ions. At the same time, the PMMA molecular in the solution embraces the ZnO nanoparticles. On the other hand, the crude ZnO nanoparticles can aggregate together

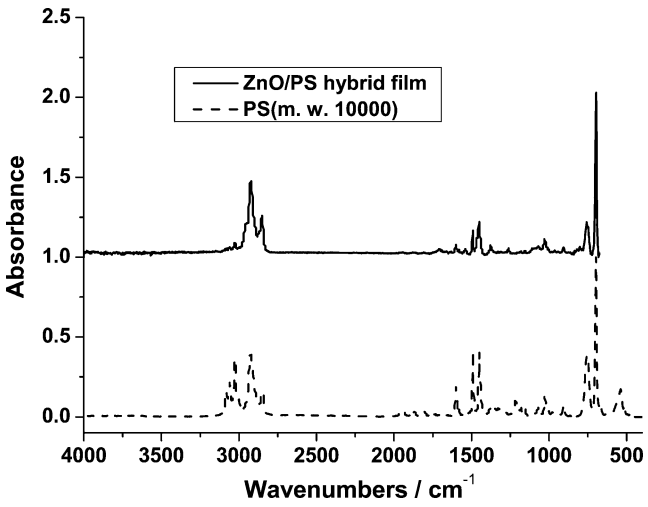

Fig. 4 FTIR spectra of the ZnO/PS hybrid film and PS from library of HR Aldrich FTIR collection edition II

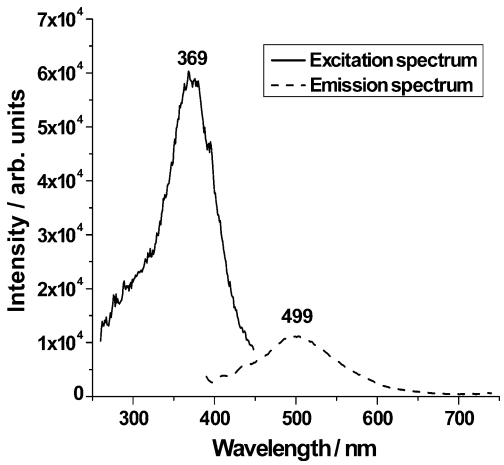

Fig. 6 Fluorescence spectrum of the ZnO/PS hybrid film

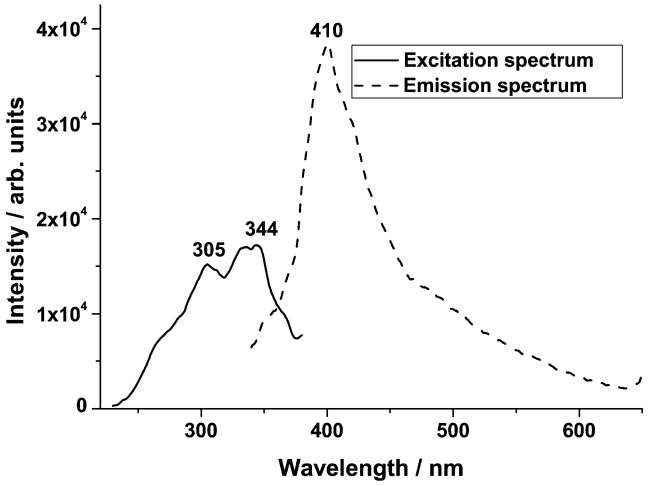

Fig. 7 Fluorescence spectrum of the ZnO–PMMA film prepared by blend process

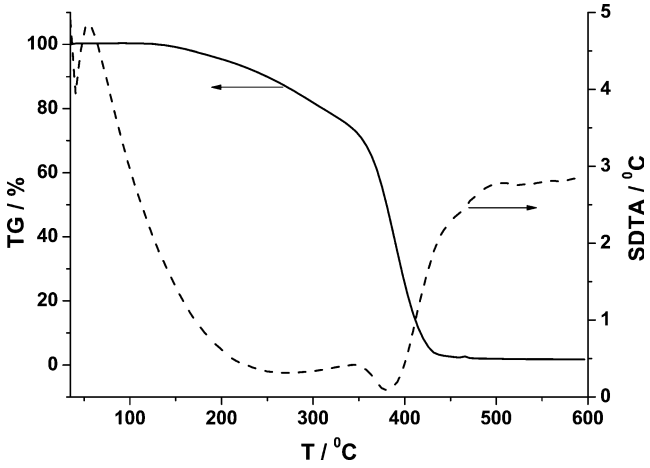

Fig. 9 TG-SDTA curves of the ZnO/PMMA hybrid film

to form bigger particles and reduce surface activity. The surface zinc ions in the aggregated particles cannot coordinate with C=O in the PMMA due to low surface activity. Thus, there are two kinds of ZnO particles formed in the ZnO/PMMA hybrid film.

Figure 6 shows the fluorescence spectrum of the ZnO/PS hybrid film. As can be seen from the figure, there is a strong broad excitation peak at 369 nm that can be attributed to the π→π* transition of the PS, and a broad emission peak at 499 nm that can be attributed to the oxygen vacancy [16, 17]. Compared to fluorescence spectrum of the ZnO/PMMA hybrid film, the excitation and emission peaks of the ZnO/PS hybrid film shift to blue and red, respectively, which indicates that polymer has great influence on the fluorescence properties of the ZnO particles due to strong interaction among ZnO nanoparticles and polymer.

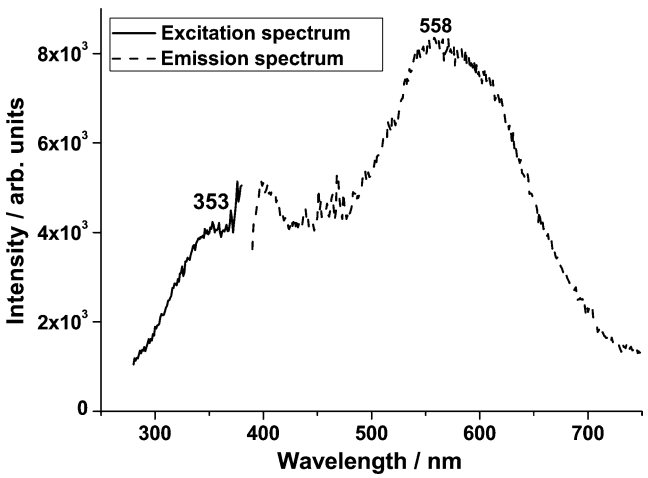

Fig. 8 Fluorescence spectrum of the ZnO–PS film prepared by blend process

In order to investigate the influence of preparing method to fluorescence spectrum, the ZnO–polymer films were prepared by blend process. Figure 7 shows the fluorescence spectrum of the ZnO–PMMA film prepared by blend process. As can be seen from the figure, there are two excitation peaks in 305 and 344 nm, one emission peak in 410 nm, respectively. These two excitation peaks can be attributed to electron transition of the ZnO particles [11], and the emission peak is believed to be excited emission of electron-hole plasmon composite [15]. When the absorption energy is higher than the energy of the forbidden band (3.37 eV), the electronic transitions from valence bands to conduction bands are enhanced, which results in the formation of electron-hole pairs.

Figure 8 shows the fluorescence spectrum of the ZnO–PS film prepared by blend process. It is found that there is an

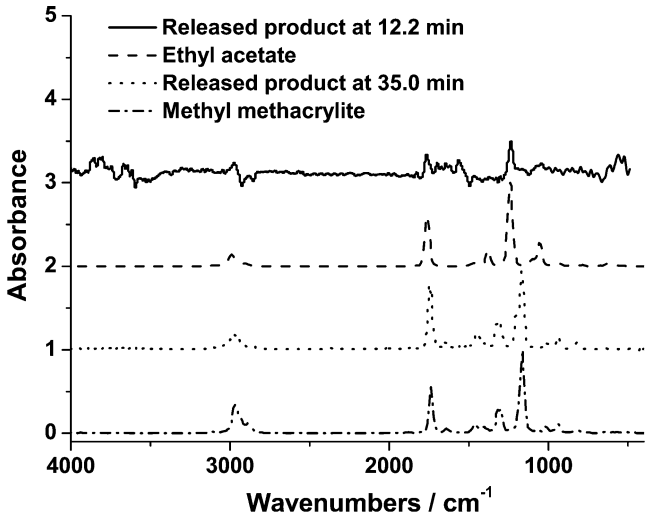

Fig. 10 FTIR spectra of the released thermal products from the ZnO/PMMA hybrid film at 12.2, 35.0 min, and standard FTIR spectra of ethyl acetate and methyl methacrylate library of Aldrich condensed phase supplement

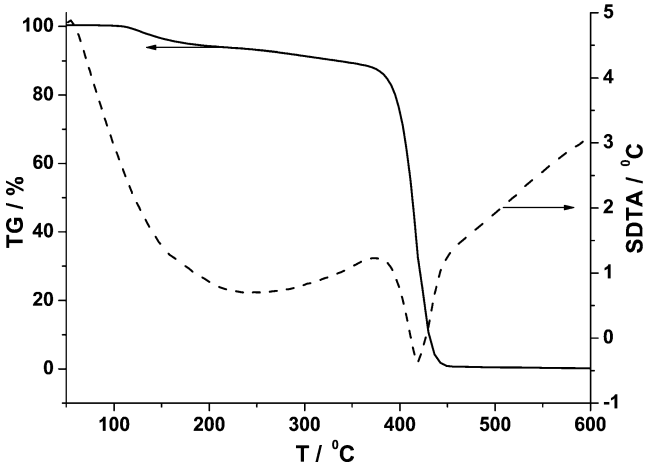

Fig. 11 TG–SDTA curves of the ZnO/PS hybrid film

excitation peak in 353 nm and an emission peak in 558 nm. Similarly, the excitation peak in 353 nm can be attributed to transition of ZnO particles. Because the pure PS has only an emission peak at 406 nm with the FWHM of 65 nm [18], the emission peak in 558 nm is not from PS. Thus, the emission peak can be contributed to the transition of ZnO particles that is related to oxygen vacancies [16, 17]. Compared to that of ZnO–PMMA film, the emission peak of ZnO particle shifts to red. This red shift may be explained by the formation of aggregates or crystals that promote formation of excimers or ground-state complexes [19].

From the above results, conclusions can be obtained that preparing methods and the interaction between ZnO particles and polymer have great influence on the fluorescence properties of the ZnO hybrid films. As ZnO nanoparticles prepared by pulsed laser ablation method can be decorated in situ and enwrapped by the polymer, the aggregation of the nanoparticle can be prevented, and the nanoparticles are distributed evenly in the polymer matrix.

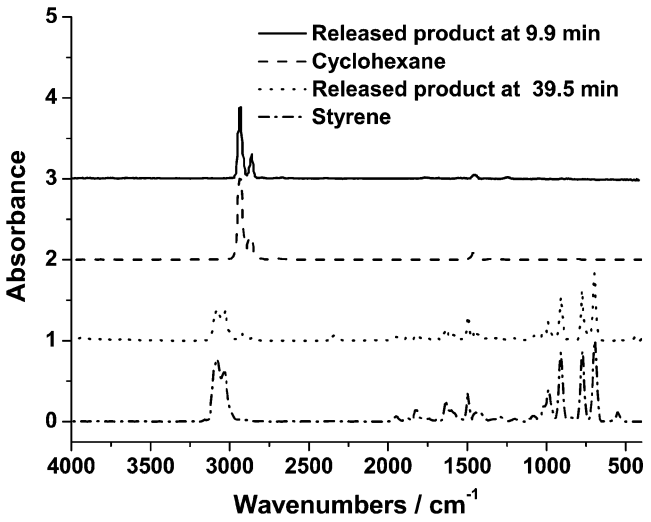

Fig. 12 FTIR spectra of the released thermal products from the ZnO/PS hybrid film at 9.9, 39.5 min, and standard FTIR spectra of styrene and cyclohexane spectrum from library of flavors and fragrances

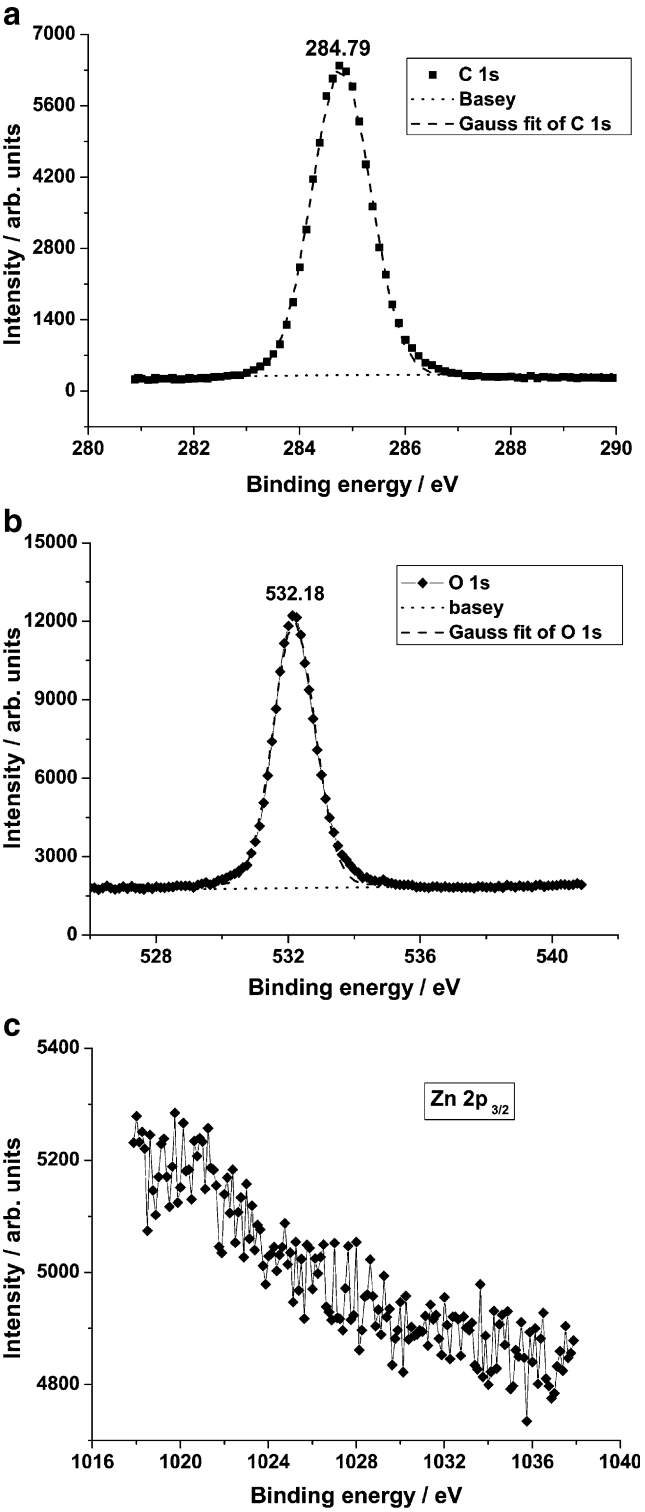

Fig. 13 XPS of the ZnO/PMMA hybrid film for C 1s (**a**), O 1s (**b**), and Zn $2p_{3/2}$ (**c**)

TG-FTIR analysis of the ZnO hybrid film

Figure 9 shows the TG/SDTA curves of the ZnO/PMMA hybrid film. In heated process, accompanying the weight loss, some materials are released at the temperatures of 125–200 °C and 300–450 °C, which can be detected by the OMNIC Series software. Figure 10 shows FT-IR spectra of the released thermal products at 12.2, 35.0 min, and standard FT-IR spectra of ethyl acetate and methyl methacrylate from library of flavors and fragrances. As can be seen from Fig. 9, the weight loss at temperatures of 100–200 °C is 6.67% and the weight loss at temperatures of 300–450 °C is 77.78%. As reported in the literature [20], the initial weight loss is considered due to vaporization of volatiles such as trapped solvent from PMMA, and the second-stage weight loss may be due to decomposition of PMMA itself. Comparing the spectrum at 12.2 min to the standard spectrum of ethyl acetate, the released product at the initial stage is ethyl acetate. Similarly, comparing the spectrum at 35.0 min to the standard spectrum of methyl methacrylate, the released product at the second stage is methyl methacrylate. The weight of the rest of the sample is 2.06 %, and the rest of the sample is ZnO.

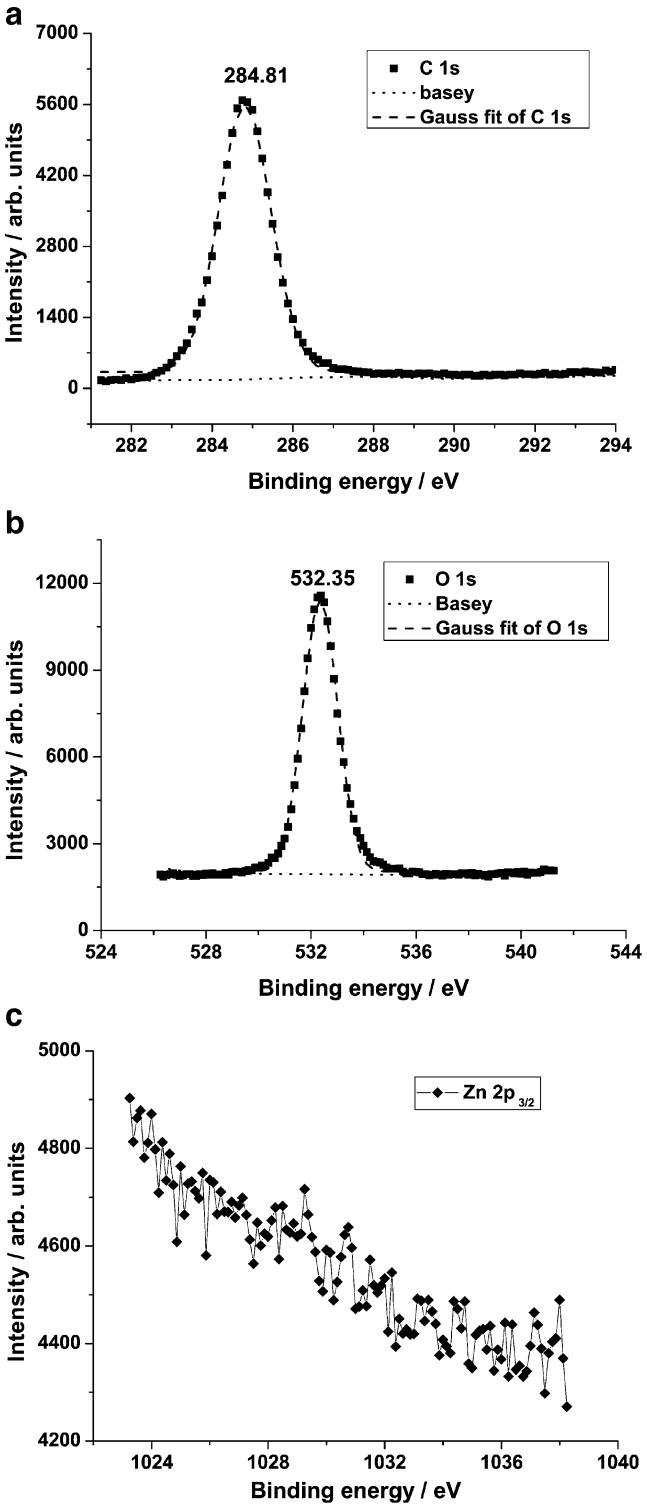

Fig. 14 XPS of the ZnO/PS hybrid film for C 1s (**a**), O 1s (**b**), and Zn $2p_{3/2}$ (**c**)

Table 1 Electron binding energies of the ZnO/Polymer hybrid films compared with those in the literature

Energy level	Electron binding energy / eV		
	The ZnO/PS hybrid film	The ZnO/PMMA hybrid film	
C 1s	284.81	284.79	284.9 [23]
O 1s	532.35	532.18	531.0 [24]
Zn 2p	–	–	1,022.1 [25]

Figure 11 shows the TG/SDTA image of the ZnO/PS hybrid film. In heated process, accompanying the weight loss, some materials are released at the temperatures of 103–167 °C and 322–450 °C, which can be detected by the OMNIC Series software. Figure 12 shows FTIR spectra of the released thermal products at 9.9, 39.5 min, and the standard FTIR spectra of cyclohexane and styrene from library of flavors and fragrances. As can be seen from Fig. 11, the weight loss at temperatures of 103–167 °C is 4.54%. Comparing the spectrum at 9.9 min to the standard spectrum of cyclohexane, the released product is cyclohexane. The weight loss at temperatures of 371–450 °C is 87.18%. Similarly, comparing the spectrum at 39.5 min to the standard spectrum of styrene, the released product is styrene. The weight of the rest of the sample is 0.90%, and the rest of the sample is ZnO.

The weight loss of pure PS is more than 90% at a temperature of 400 °C [21]. In the ZnO hybrid film, the weight loss of PS is about 24.2 % at a temperature of 400 °C. The weight loss of pure PMMA is about 25% at a temperature of 303.8 °C [20, 22], and the weight loss of the ZnO/PMMA hybrid film is 20.7% at the same temperature. As a result, the ZnO/polymer hybrid films have better thermostability than the related pure polymers.

XPS analysis of the ZnO/polymer film

The results of the XPS analyses for the ZnO/PS and ZnO/PMMA hybrid films are shown in Figs. 13 and 14, respectively, which show the scan for Zn 2p, O 1s, and C 1s in the ZnO/polymer hybrid film. The peaks read from these XPS spectra are given in Table 1, together with results reported in the literature [23–25]. As can be seen from Table 1, C 1s and O1s of the hybrid films can be detected by XPS, where there is a decrease of 1.18–1.35 eV for the binding energy of O 1s electrons compared to that of ZnO reported in the literature [25], which indicates existence of polymer influences the microenvironment of Zn^{2+} ions. Furthermore, the binding energy of O 1s in the ZnO/PMMA hybrid film has an increase of 0.17 eV than that in the ZnO/PS hybrid film. The main reason is that the C=O in PMMA can coordinate with surface Zn^{2+} of the ZnO nanoparticles and form delocalized π bond, which results in decrease of bonding energy of O 1s [26]. Because the ZnO nanoparticles are enwrapped by polymer, and XPS can only detect the area 10 nm under sample surface, the Zn 2p in two kinds of hybrid films cannot be detected by XPS.

Conclusion

The cyclohexane solution of PS and the ethyl acetate solution of PMMA were used as flowing liquid; the ZnO/polymer colloids were successively produced by focused pulsed laser ablation of ZnO target in interface of solid and flowing liquid. The obtained ZnO/polymer hybrid colloids were condensed and then dropped on the glass. As solvent in the hybrid colloids has volatized, the ZnO/polymer hybrid films were obtained. HRTEM, SEAD, fluorescence spectrum, FTIR spectroscopy, TG-FTIR, X-ray photoelectron spectrum were used to characterize the hybrid films. HRTEM results show a good dispersion of ZnO nanoparticles in the polymer matrix. The fluorescence spectrum of the ZnO/PMMA hybrid film exhibits a broad emission peak at 489 nm and a weak emission peak at 424 nm; the fluorescence spectrum of the ZnO/PS hybrid film exhibits a broad emission peak at 499 nm. The emission peak at 424 nm can be attributed to electron-hole plasma recombination emission of nano-ZnO particles, and the emission peaks at 489 and 499 nm can be attributed to the recombination of a photogenerated hole with the singly ionized charge state of the defect, respectively. XPS cannot detect the Zn 2p of the ZnO/polymer hybrid films, which indicate the ZnO nanoparticles were enwrapped by the polymers; this wrap makes the ZnO nanoparticles isolate from the atmosphere. Thus, the ZnO/polymer hybrid films have higher chemical stability than ZnO nanoparticles. In addition, the ZnO/polymer hybrid films have better thermostability than that of the related pure polymers because of strong interaction among ZnO particles and polymers.

Acknowledgement The authors are indebted to the financial support of the National Natural Scientific Foundation of China (No.50272014), the Key Nano Special Item of Fujian Province of China (No.2005HZ01-5), Natural Scientific Foundation of Fujian Province of China (No. A0710001) and the Education Department of the Fujian Province of China (No. JB07061).

Reference

1. Lima SAM, Cremona M, Davolos MR, Legnani C, Quirino WG (2007) Thin Solid Films 516:165
2. Kligshirn C (1975) Phys Status Solidi B 71:547
3. Numerical Data and Fundamental Relationships in Science and Technology, Vol. 17 of Landolt–Bornstein new series, Springer-Verlag, Berlin, 1982
4. Kang JS, Kang HS, Pang SS, Shim ES, Lee SY (2003) Thin Solid Films 443:5
5. Millers D, Grigorjeva L, Łojkowski W, Strachowski T (2004) Radiat Meas 38:589
6. Li XH, Yuan QL, Wang DN, Ying SK (2000) J Funct Polym 13:211
7. Zhang WG, Zhang Y, Tang JY, Wang LH, Ling QD (2002) Thin Solid Films 417:43
8. Chen QH, Zhang WG (2007) J Colloids Interface Sci 309:531
9. Chen QH, Zhang WG (2007) Appl Surf Sci 253:3751
10. Chen QH, Zhang WG, Huang XX (2007) J Lumin 126:309
11. Chen QH, Zhang WG (2007) J Non-Cryst Solids 353:374
12. Chen QH, Zhang WG, Huang XX (2008) Opt Mater 30:822
13. Compagnini G, Scalisi AA, Puglisi O (2002) Phys Chem Chem Phys 4:2787
14. Sun J, Akdogan EK, Klein LC, Safari A (2007) J Non-Cryst Solids 353:2807
15. Bagnall DM, Chen YF, Zhu Z, Yao T (1997) Appl Phys Lett 70:2230
16. Vanheusden K, Warren WL, Seager CH, Tallant DR, Voigt JA (1996) J Appl Physi 79:7983
17. Chen HS, Qi JJ, Huang YH, Liao QL, Zhang Y (2007) Acta Phys-Chim Sin 23:55
18. Wang W, Lin MJ, Zhang WG (2004) Chinese Journal of Applied Chemistry 21:286
19. Papadimitrakopoulos F, Zhang XM, Thomsen DL, Higginson KA (1996) Chem Mater 8:1363
20. Khanna PK, Singh N (2007) J Lumin 127:474
21. Kogler FR, Schubert U (2007) Polymer 48:4990
22. Lin MJ, Zhang WG, Wang W (2002) J Chin Rare Earth Soc 20:97
23. Clark DT, Kilcast D, Adams DB, Muagrave WKR (1972) J Electron Spectrosc Relat Phenom 1:232
24. Strohmeier BR, Hercles DM (1984) J Phys Chem 88:4922
25. Gaarenstroom SW, Winograd N (1977) J Chem Phys 67:3500
26. Drabold DA, Adams JB, Anderson DC, Kieffer J (1993) J Adhes 42:55